DOI 10.4430/bgo00377

# Application of geophysical and geological analyses to identify the main karst conduit close to the Sarabegarm spring, west Iran

M. Mozafari [1], M. Moradi [2], M. Javad Bolourchi [3], A. Aliyari [3] and M. Sajjadian [4]

[1] *School of Geology, College of Science, University of Tehran, Iran*

[2] *Institute of Geophysics, College of Science, University of Tehran, Iran*

[3] *Zamin Ab Pey Consulting Engineers Company, Tehran, Iran*

[4] *Iran Ministry of Energy, Tehran, Iran*

(Received: 23 March 2021; accepted: 28 September 2021; published online: 3 December 2021)

***ABSTRACT*** The Sarabegarm karstic spring is located near the NW plunge of the Danehkhoshk anticline in western Iran. The spring is the main source of drinking water in the region, therefore understanding the path and location of its main karst conduit is crucial to protecting it from the risk of contamination. Near the spring, karstic limestone was dissected by two main sets of tension joints with N20E and N30W direction. The Mise-A-La-Masse (MALM) investigation showed that the main direction of groundwater flow towards the spring was elongated about N25E, almost coinciding with the surface trace of the NE trending fractures. The 2D frequency-domain induced polarisation surveys indicated that the zones with low resistivity and chargeability values were located below the trace of two main fractures. Since the main conduit system of the spring was most likely developed in the crushed zones of these fractures, the area near them has the highest vulnerability and must be protected from any activity posing a risk of contamination. Results of this study showed that the application of frequency domain electrical resistivity, in combination with the geological analysis, could be suitable in characterising the shallow main conduits, particularly in the vicinity of big karst springs.

**Key words:** Sarabegarm spring, karst conduit, geophysical methods, Mise-A-La-Masse, electrical resistivity tomography.

## 1. Introduction

Karst terrains are usually known by complex geological features and unique hydrogeological characteristics. Karst aquifers are characterised by three types of porosity: matrix (or intergranular), fracture, and conduits (Martin and Screaton, 2001; Ford and Williams, 2007). Matrix porosity is important in providing storage capacity for the aquifer; conversely, fracture and conduit porosity provide pathways for groundwater flow (White, 2007). Laminar or slow flow arises through the matrix or narrow fractures, and turbulent or rapid flow occurs within the connected fractures or conduits (Palmer, 1991; Ford and Williams, 2007). Springs represent the output of karst systems and exerte considerable control on groundwater flow through aquifers. The diffuse or concentrated water recharge is finally transmitted to conduit networks, which are extended like a plumbing system through the aquifer and into the springs (White, 2007).

© 2022 - OGS

Detecting the route and location of the main conduits terminating at the springs is essential in developing solution strategies against specific problems such as karst water pollution (Green *et al*., 2006; Kalhor *et al*., 2019), leakage from dam sites (Mozafari and Raeisi, 2015, 2016; Milanović, 2018; Mozafari *et al*., 2021) and water inrush during tunnel construction (Alija *et al*., 2013). Although a great majority of conduits is guided by bedding planes, joints and faults, determining the location and direction of conduits presents significant practical problems due to the severely anisotropic and heterogeneous nature of karst aquifers (Palmer, 1991; Ford and Williams, 2007; White, 2007). However, accessible caves and shafts sometimes provide the opportunity to make direct observations in small parts of a karst conduit.

Borehole analysis (coring and bore video logging) and tracing tests are the main conventional methods to detect conduit locations and paths. There is a significant practical problem in location utilising borehole investigations or tracing tests. Numerous boreholes are needed to find suitable data on conduit passages and it is virtually impossible to acquire sufficient data on a conduit route with only a few boreholes. Moreover, only few boreholes encounter the major karst conduits as the areal coverage of conduits is usually less than 1% of the aquifer area (Worthington, 1999). Tracer tests are powerful tools to find hydraulic relationships between the recharge and discharge points and, therefore, estimate the rate of water movement through a conduit system. It is rarely possible to demonstrate the location and path of karst conduits by tracer tests without drilling numerous boreholes and doing frequent water sampling (Mozafari *et al.*, 2018).

In recent decades, geophysical methods have been widely used in karst studies. The electrical resistivity method has been used to establish the base of karst as a technique to distinguish between compact, dry and water saturated karstic limestone (Beres, 2013; Redhaounia *et al*., 2016; Pazzi *et al*., 2018; Cheng *et al*., 2019). Microgravitational methods were often applied to detect shallow subsurface karst due to missing mass over caves and conduits (McGrath *et al*., 2002; Debeglia *et al*., 2006; Chalikakis *et al*., 2011). Furthermore, Ground Penetrating Radar (GPR) was widely used to detect the near-surface karst, particularly related to the subsidence and sinkholes (Al-Fares *et al*., 2002; Zarroca *et al*., 2017). Moore and Stewart (1983), Zhu *et al*. (2011) and Gan *et al*. (2017) have used multi-geophysical approaches to detect underground karst channels and find signatures of fracture traces in the karst aquifers. It should be noted that any geophysical technique has its limitations, especially with respect to the size and depth of karst features, thickness of soil cover and ground topography (Ford and Williams, 2007). Bakalowicz (2005) stated that almost no geophysical technique was suitable for locating conduits at depths greater than 40 to 50 m. The most successful sites for geophysical investigations are likely to be close to permanent karst springs where conduits become sufficiently enlarged to transmit significant volumes of water.

The Sarabegarm spring is located about 5 km SW of Sarepolezahab city, west Iran (Fig. 1). The spring provides drinking water for the cities of Sarepolezahab and Qasreshirin, respectively with populations of about 85,000 and 25,000. As part of the drinking water safety plan, the whole catchment area of the spring, including the route of its main conduit, should be protected from all activities posing a risk of contamination (e.g. farming, grazing, burning, road construction, building, use of chemicals, etc.). Therefore, understanding the route and location of the main conduit was fundamental. To this end, an attempt has been made to delineate the location and route of the main karst conduit towards the Sarabegarm spring using a combination of geological and geophysical investigations.

## 2. Geological setting and hydrogeological framework

The study area is located at the Simple Folded Zagros zone, west Iran (Fig. 1a). At the Zagros zone, anticlines are generally cylindrical in form and well-exposed as high mountains, while the synclines form valleys and plains (Miliaresis, 2001; Saein, 2018). The geological map of the study area, including the main geological structures and distribution of formations and faults at the region, is shown in Fig. 1b. The Danehkhoshk anticline (Fig. 1c), NW-SE oriented, parallel to the general trend of the Zagros zone, is the main geological structure in the area. Geometrically, the fold shows a cylindrical form, which plunges down at both ends. The main rock units exposed at the study area include (Fig. 1b): about 900 m shale and marlstone of Pabdeh-Gurpi Formation (Cretaceous-Tertiary), near 360 m thick limestone of Asmari Formation (Oligo-Miocene), about 2,000 m evaporites and marlstone belonging to the Gachsaran Formation (Tertiary), and about 1,000 m conglomerates and sandstone of the Bakhtiary Formation (Tertiary). These formations are mostly exposed at the highlands and hills, while the Quaternary deposits are mainly exposed at the adjacent plains and residential areas (Figs. 1b and 1c).

At the Danehkhoshk anticline, the Asmari Formation forms a karst aquifer, whereas the impermeable Pabdeh-Gurpi Formation forms the bedrock (Figs. 1b and 2c). Karren, grike, cave, and springs were the main surface karst features of the aquifer. Karren with different sizes and shapes, including rainpits, rillenkarren, and grikes, are well-developed in the limestone and distributed at all elevations. Grikes up to 1 m wide and several metres deep were well-developed along some of these joint systems, exposed particularly on near vertical walls. Caves, several metres in width and depth, are exposed in various locations on the karst limestone.

The Sarabegarm spring emerged from the Asmari Formation, near the NW plunge of the Danehkhoshk anticline (Figs. 1b and 1c), where the bedding planes dip at 20° to 30° to the NE and strike N45W. The spring emerged along the boundary of limestone with alluviums (Fig. 1c). The recharge source of the Asmari aquifer is direct rainfall on the aquifer surface. There is no recharge from the surrounding impermeable Gachsaran Formation and alluvium, since they are located at lower elevations. After entering to the karst aquifer, groundwater flows through the aquifer body and finally discharges through the Sarabegarm spring.

The changes in the rainfall and spring discharge during 2007 to 2018 are presented in Fig 2. A rise in spring discharge can be observed during the years with intense rainfall events, but spring discharge did not vary significantly over a year and minimum discharges never drop below 1,100 l/s, despite the low rainfall in some years. To identify karst aquifer characteristics, recession curves of the spring hydrographs were analysed. Semi-logarithmic plots of recession curves are often expressed by (Ford and Williams, 2007; Li *et al*., 2016):

$$Q_t = Q_0\, e^{-\alpha t} \tag{1}$$

where $Q_t$ is the discharge ($m^3s^{-1}$) at time $t$, $Q_0$ is the initial discharge at time zero, $t$ is the time elapsed (usually expressed in days) between $Q_t$ and $Q_0$, $e$ is the base of the Napierian logarithms and α is termed the recession coefficient. By plotting the recession curves of the spring hydrograph on the logarithmic ordinate, based on the data collected during 2016, one straight line was acquired. The calculated recession coefficients values, $\alpha_1$, were 0.0007 ($day^{-1}$).

Results of physico-chemical characteristics of spring water samples are given in Table 1. The electrical conductivity of water during the measured years varied from 490 to 555 µs/cm

and the ion concentration changed slightly through the year. The Ca-$HCO_3$ was the dominant type of water samples, whereas the $Ca^{2+}$ and $HCO_3^-$, respectively, contributed more than 46 and 83% to the cation and anion budgets of water samples. The competed saturation indices for calcite indicated that all water samples were under-saturated with respect to this mineral. The low recession coefficient of the spring hydrograph, together with the slight hydro-chemical variations, indicated that the discharge of the spring consisted mostly of base flow during a year.

Table 1 - Parameters of water samples collected from the Sarabegarm spring (Iran Water Resources Management Company, 2020).

| Date | Discharge (l/s) | Electrical conductivity (µs/cm) | pH | Cations (meq/l) | | | | Anions (meq/l) | | | | Calcite saturation index |
|---|---|---|---|---|---|---|---|---|---|---|---|---|
| | | | | Ca | Mg | Na | K | Cl | $SO_4$ | $HCO_3$ | $CO_3$ | |
| 06 Aug 1985 | 1900 | 555 | 7.50 | 3.2 | 1.5 | 0.23 | - | 0.27 | 0.30 | 4.35 | - | -2.1 |
| 16 May 2017 | 2326 | 494 | 7.21 | 2.8 | 1.9 | 0.12 | - | 0.20 | 0.60 | 4.00 | - | -2.5 |
| 08 Jun 2017 | 2060 | 490 | 7.61 | 2.7 | 2.0 | 0.10 | - | 0.20 | 0.37 | 4.20 | - | -2.1 |

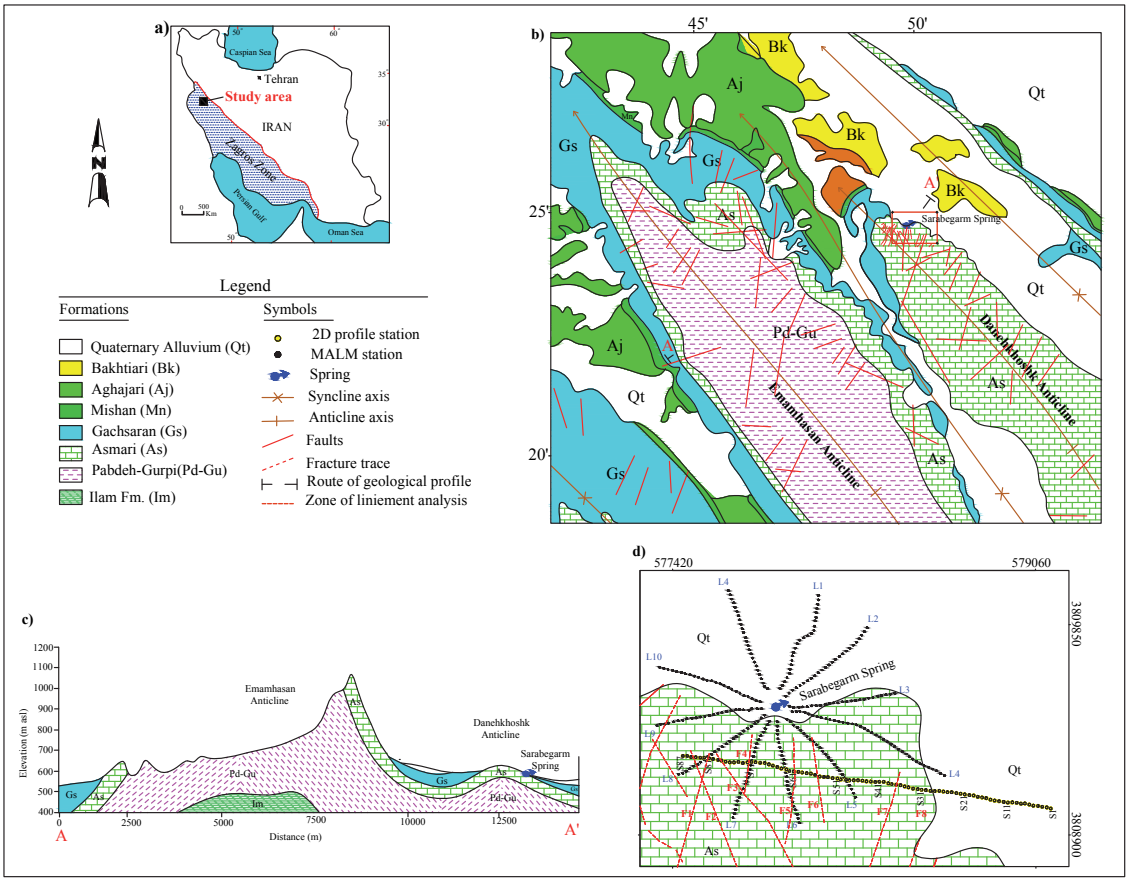


Fig. 1 - The study region: a) location of the study area on the map of Iran and Zagros zone; b) geological map of the study area (modified after Iranian National Oil Company, 2006); c) cross-section along the Emamhsan and Danehkhosk anticlines (the route of this cross-section is shown in Fig. 1a); d) the route of the geophysical profiles measured in the study area. L1 to L11 show the MALM profiles and S1 to S87 show the 2D profile stations.

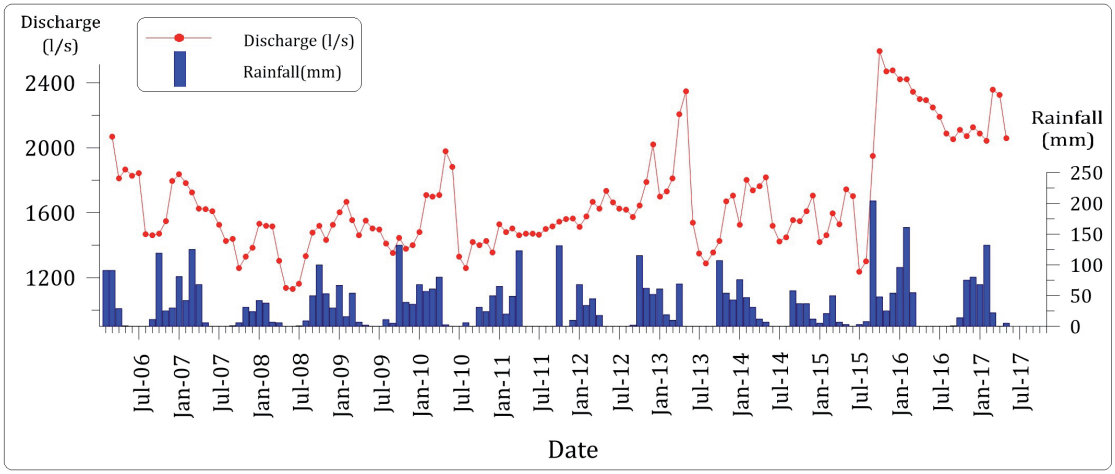


Fig. 2 - Time series of precipitation and Sarabegarm spring discharge, based on the data of Iran Meteorical Organization (2020) and Iran Water Resources Management Company (2020).

## 3. Material and methods

To find the location and path of the main karst conduit near the Sarabegarm spring, in an area about 1 km in diameter around the spring (Fig. 1d), geological and geophysical surveys were conducted. The structural and geomorphic data on the Asmari Formation was collected during the field work. The dip and strike of bedding planes and the fault and major joint systems were determined and mapped. The initial map was completed with a handheld GPS (global positioning system) device during the field work. These tests resulted in a fracture trace lines map, which shows the location and path of zones suitable for conduit development. The resulting map was checked by aerial images to enhance the fracture data coverage and accuracy.

The Mise-A-La-Masse (MALM) method (also called excitation at the mass), along with the 2D frequency-domain induced polarisation, was applied at the study area to track the underground water flow towards the Sarabegarm spring. For data collection of both methods, a set of portable geoelectric equipment, including an ASTRA-100 generator and a MERI-24 meter was used. The ASTRA-100 is a portable generator, which provides an alternating low frequency current. The MERI-24 is a multifunctional electromagnetic receiver, which supports a wide range of frequency, from 0.15 to 625 Hz. The signal-to-noise ratio of measurements could be improved by applying the low frequency alternating currents and considering that: a) in case of long electrode spacing, it was necessary to control the near zone conditions adjacent to the current line since the measured data was affected by an induction component of the electrical field; and b) it was needed to avoid the inductive effect between the transmitter and receiver wires due to use of an alternative current by applying the low frequency alternative current (Kulikov *et al.*, 2013).

MALM is a useful technique for mapping the highly conductive subsurface bodies. For this method, the conductive mass under investigation is used as one of the current electrodes and the second current electrode is placed at a large distance away. The potential distribution from these two current electrodes would be expected to yield some information about the continuity, extent, dip, and strike of the conductive mass (Wightman *et al.*, 2003; Kulikov *et al.*, 2013). At the study area, the MALM method was applied in a frequency domain with a frequency of 0.61 Hz. Here, the resistivity measurements were done along 11 radial profiles (L1 to L11 in Fig. 1d) with an average angle of 30°. In order to increase the signal-to-noise ratio, the transmitted

current was increased by enlarging the distance to the spring. Therefore, measured voltage at the potential electrodes was normalised by injected current. The electromagnetic coupling effect was decreased by applying the low frequency (0.61 Hz) injected current and using a short connected cable between the potential electrodes and the receiver. The electrical current was injected into the ground using the point source electrodes and the results were presented simply as a map of normalised voltage by current values.

In the frequency-domain induced polarisation method, an alternating current with variable frequencies is injected into the ground, and then the voltage phase-shifts must be measured to evaluate the impedance spectrum at the different injection frequencies (Zonge *et al*., 2005). The principle of this method consists of the phase shift measurement between the harmonic waves of a square pulse recorded in the receiving line. The differential phase parameter ($\Delta\varphi$) could be calculated by the phase shifts (Kulikov *et al*., 2013):

$$\Delta\varphi = [\omega_2\varphi_1 - \omega_1\varphi_2]/[\omega_2 - \omega_1] \quad (2)$$

where the $\omega_1$ and $\omega_2$ are respectively the high and low frequencies (2.44 and 0.61 Hz in this study) and the $\varphi_1$ and $\varphi_2$ are respectively phase shift between the injected current (at the current electrode) and measure potential (at the potential electrode) for the different harmonic waves.

The measured signal was proportional to the apparent polarisation, $\eta_{ap}$ = -2.5$\Delta\varphi$. Good noise protection, especially in urban areas, and suppression of phase shifts caused by the electromagnetic coupling are known as the main advantages of the phase frequency method (Kulikov and Shemyakin, 1978). Another important point in frequency domain investigation is related to the capacitive leakage from the current line to the earth or directly into the receiving line. The capacitive leakage value is directly proportional to the current line resistance, which mostly depends on the current electrode grounding resistance. Resistance between current electrodes should be less than 10,000 Ω. It should be mentioned that the higher resistance of receiver electrodes could negatively affect the induced polarisation measurement. So, resistance between the receiver electrodes should be less than 5,000 Ω. Such being the case, the ASTRA-100 generator could be used to measure the receiving and transmitter line resistance, because it could be applied as an ohmmeter due to its special integrated function.

In this study, the frequency-domain induced polarisation was measured along a 2D profile to find the conduit's locations precisely. The 2D profile was spread in a west to east direction, perpendicular to the main geo-electrical strike, which was detected by the MALM investigation. The Sarabegarm spring is located at the boundary of limestone and alluviums. Since the spring water typically comes from the adjacent elevated karst aquifer, the resistivity profile was designed to be situated mostly on the limestone to find evidence of the karst conduit (Fig. 1d). The measured stations located along a 1,740-m-long profile were named S1 to S87 by moving from the east towards the west (Fig. 1d). The resistivity and induced polarisation were measured by applying the dipole-dipole electrode configuration with a 20 m dipole length along the profile (Fig. 1d). In order to increase the signal-to-noise ratio, resistivity data were measured in frequency of 0.61 Hz. Induced polarisation values were measured with phase-frequency methods in frequencies of 0.61 to 2.44 Hz. Finally, the measured data were inverted by the smoothness constrained least-squares approach in the Res2DInv Software, according to the method applied by Loke (2010). The inversion was terminated by seven iterations since the roote mean square value (RMS) was decreased to below three percent for both resistivity and chargeability model.

## 4. Results

The fracture trace lines map provided by the field mapping is shown in Fig. 3. In the analysed zone with an area of about 1.5 km$^2$, the cumulative length of the fractures mapped was 9.4 km with the fractures having an average length of 300 m. As can be seen in Fig. 3, two dominant tension joint systems were extended at the Asmari Formation. The first joint system had a N20E trend, while the second showed a N30W trend. It was difficult to measure dip direction of fractures in depth because they were filled with unconsolidated sediments. The designed 2D resistivity profile dissected seven major fractures, named F1 to F8, by moving from the west to east (Fig. 3). The measured length of the F1, F2, F3, F4, F5, F6, F7, and F8 fractures were respectively 690, 1,610, 1,220, 1,110, 400, 550, 410, and 2,100 m. The F4 and F5 fractures were connected to the F2 fracture at their SE ends. Except the F1, F2, F3, and F8 fractures with several metres opening, the widths of the other fractures were less than 1 m.

The result of the MALM survey in the study area is presented as a map of normalised current to the potential values (Fig. 4). Flow through conduits towards the springs provided an underground pathway of electrical current perpendicular to the iso-potential contours. The map showed that the iso-potential contours were almost elongated toward N25E from the limestone to the adjacent alluvium, almost connected to the trace of the F3 and F4 fractures (Fig. 4).

The results of the inverted resistivity and chargeability measured at the site are respectively shown in Figs. 5a and 5b. To understand the relation between resistivity and lithology, the sediment resistivity probability curve was provided using the measured data (Fig. 6) and according to a processing procedure found in Shevnin *et al*. (2006a, 2006b) and Hunter and Crow (2015). The correlation between resistivity and lithology indicated that resistivity values lower than 100 Ω·m were related to the unconsolidated sediments (alluvium), whereas values higher than 200 Ω·m were associated to the rocks belonging to the Asmari Formation. Therefore, the

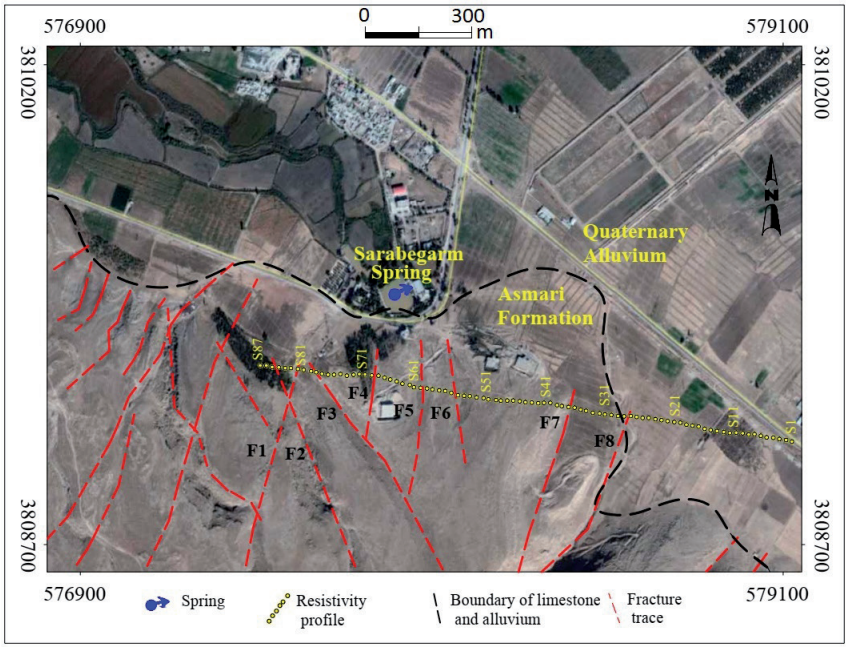


Fig. 3 - The fracture trace map acquired from field data. The route of the 2D profiles are shown along the S1 to S87 stations.

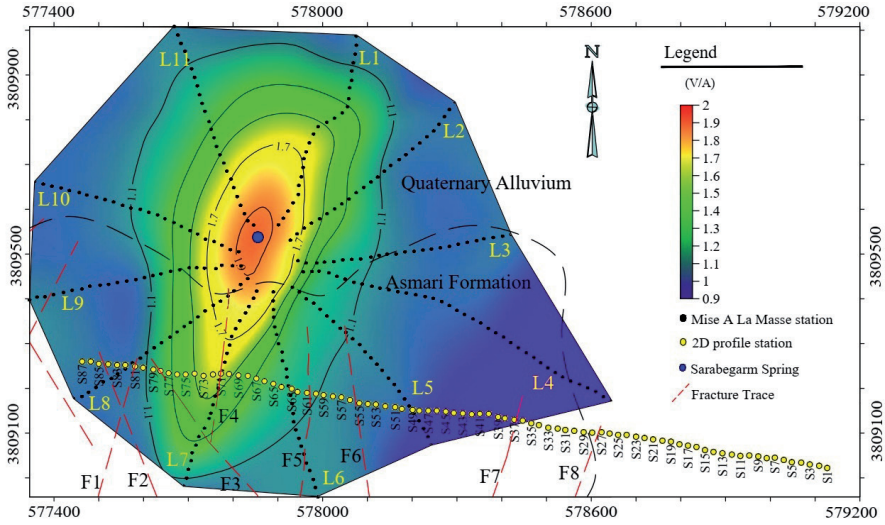


Fig. 4 - Map of iso-potential counter based on the MALM investigation.

S35 station could be considered as the boundary of limestone and alluvium (Fig. 5a). Since the Sarabegarm spring was recharged from the Asmari Formation, clustering resistivity of limestone was very important to delineate water filled karstified limestone. The theoretical porosity-resistivity curves for carbonate rocks with different clay and sand percentages were produced by the Petrowin program (Ryjov and Sudoplatov, 1990).

The selected parameters for the theoretical model of the Asmari Formation are shown in Table 2. Despite the fact that the minor effect of clay particles was found in the chargeability section and also the maximum measured total dissolved solid (TDS) of water samples from Sarabegarm spring was less than 250 mg/l, a wide range of clay percent and TDS values was considered in theoretical cross-plots (Fig. 7). As can be seen in Fig. 7, the total porosity of pure limestone belonging to the Asmari Formation was considered to be about 20%. At this condition, the bulk resistivity value for the saturated limestone could not be decreased up to 200 Ω·m by TDS value between 160 to 250 mg/l. It shows that decreasing the resistivity of pure limestone to less than 200 Ω·m required the contribution of at least 30% clay to be mixed with the limestone and/or increasing the porosity of limestone to more than 20% (as a secondary porosity). Providing the chargeability map was useful in detecting the sediments including clay and silt. The high chargeability values coincided with the clay and silt bearing sediments, whereas the

Table 2 - Petrophysical parameters, which are used to calculate theoretical porosity-resistivity cross-plot for limestone belonging to the Asmari Formation.

| Row | Petrophysical parameters | Clay characteristic | Sand characteristic |
|---|---|---|---|
| 1 | Radius | 1 µm | 25 µm |
| 2 | Porosity | 50% | 20% |
| 4 | CEC | 0.5 | - |

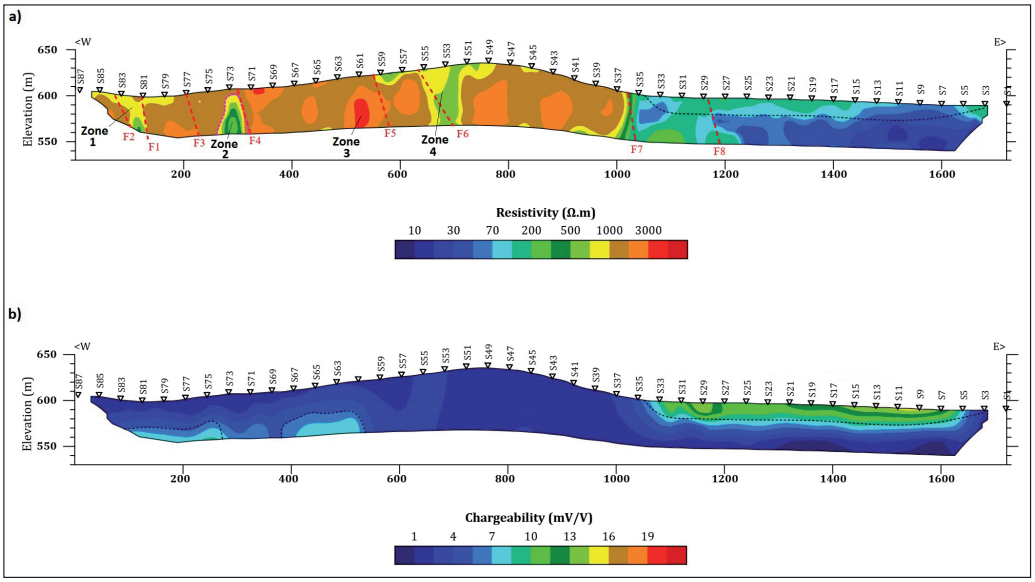


Fig. 5 - Inverted resistivity (a) and inverted chargeability (b) sections. Zones 1, 3, and 4 show the conductive anomalies and Zone 2 indicates a resistive anomaly.

low chargeability values indicated limestone. Considering the chargeability section (Fig. 5b), the S35 station could be considered as the boundary of limestone and sediments involving clay and silt. The higher chargeability values in the eastern part of the station coincided with the alluvium (bearing clay and silt), while the lower chargeability values in the western side indicated that limestone belongs to the Asmari Formation. Consequently, decreases in the resistivity could not be related to the limestone impurity by clay or silt. By comparing sections of inverted resistivity, theoretical cross-plots and geology (especially at outcrops of the Asmari Formation), the resistivity value in the Asmari Formation could be categorised in the three groups: a) water filled fractured limestone with resistivity between 200 to 700 Ω·m; b) dry or partially water filled porous or fractured limestone with resistivity about 700 to 2,000 Ω·m; and c) dry porous limestone with resistivity more than 2,000 Ω·m.

Considering the resistivity map (Fig. 5a), it was possible to observe four zones with low resistivity anomalies along the applied profile: a) Zone 1 with resistivity ranging from 700 to 1,000 Ω·m, which was located in the space between the S81 to S83 stations; b) Zone 2 with resistivity ranged from 200 to 600 Ω·m, which was situated between the S72 to S74 stations; c) Zone 3 located in the space between the S51 to S56 stations with resistivity from 700 to 1,000 Ω·m; and d) Zone 4 with about 3,000 Ω·m resistivity, situated in the space between S59 to S63 stations. The conductive zones 1 and 3 are most probably related to the partially saturated porous or fractured limestone. Zone 2 had the highest conductivity in the profile and was most probably related to water filled karst conduit or fractured limestone, located about 30 m below the ground surface. The high resistivity of Zone 4 was likely due to a relict fracture or conduit. All of these zones did not show any anomaly in chargeability values. Therefore, the zones with low resistivity in the Asmari Formation were related most probably to water bearing fractures or conduits, not associated with the presence of unconsolidated sediments. At certain points, moderate increases in the chargeability value (up to 8 mV/V) could be seen in the limestone due to the calcite dissolution and precipitation processes in fractures.

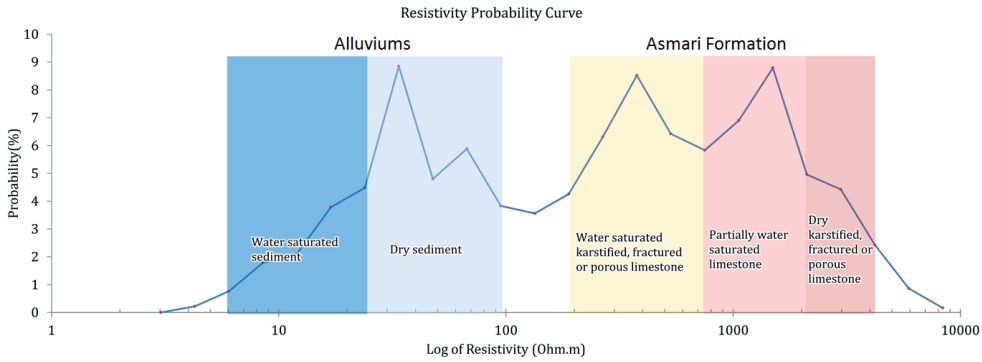


Fig. 6 - Clustering the inverted resistivity value based on the statistical analysing and geological outcrops.

## 5. Discussion

The Sarabegarm spring is the main output of the Asmari karst aquifer and has considerable control on groundwater flow through the aquifer. The spring's hydrograph presented a low $\alpha_1$, which indicated that the output of aquifer consisted mainly of slow flow through the matrix or the small fractures, except at the time of intense rainfall events. The spring water type (Ca-$HCO_3$) indicated that the limestone makes the host lithology of the flow pathways. The slight changes in ions concentration during the year showed that a huge volume of water was mainly stored in the porous matrix and small fractures in the aquifer and transmitted slowly into the main conduit near the spring. The karst conduit systems usually occupy a small portion of the total aquifer porosity. The fractures frequently direct the predominant conduit route in a karst aquifer since the zones with high permeability and low strength have aligned along them. It is difficult to detect the dip direction of fractures in depth based on their surface traces, but shallow karst conduits are usually located around the corresponding fracture traces. Therefore, one of the F1 to F7 fracture traces near the Sarebegarm spring most probably belongs to the main conduit of the spring. Considering distance to the spring, the F4 and F5 fractures have a higher chance than other fractures of being the trace of the main conduit toward the spring. However, the further geophysical investigations helped find the target fracture. The MALM map shows that the groundwater through the limestone was elongated N25E toward the spring (Fig. 4). In limestone, groundwater flowed in the space between the F3 to F4 fractures but it was distributed after reaching the alluviums (Fig. 4). This evidence showed that the main conduit system of the spring most likely developed in the crushed zone of F3 and F4 fractures. It should be noted that the resulting MALM map displayed a comprehensive view from depth up to the ground surface and, therefore, a general trace of water flow toward the spring.

The results of resistivity were useful to delineate the target conduit with more certainty. The depth and shape of conduit could be evaluated to some extent by the 2D resistivity and chargeability sections. The 2D resistivity and induced polarisation survey showed that the lowest resistivity and chargeability values at the limestone coincided with Zone 2, most likely corresponding to the main water filled karst conduit at the site. This zone, with about 20 to 50 m depth, was extended in the space between the S71 to S75 stations in the area between the F3 and F4 fractures. The F3 fracture, with 1,220 m length, has a NW trend, while the F4 fracture, with 400 m length, is extended toward NE, almost parallel to the groundwater elongations acquired by the MALM investigation. The F4 fracture

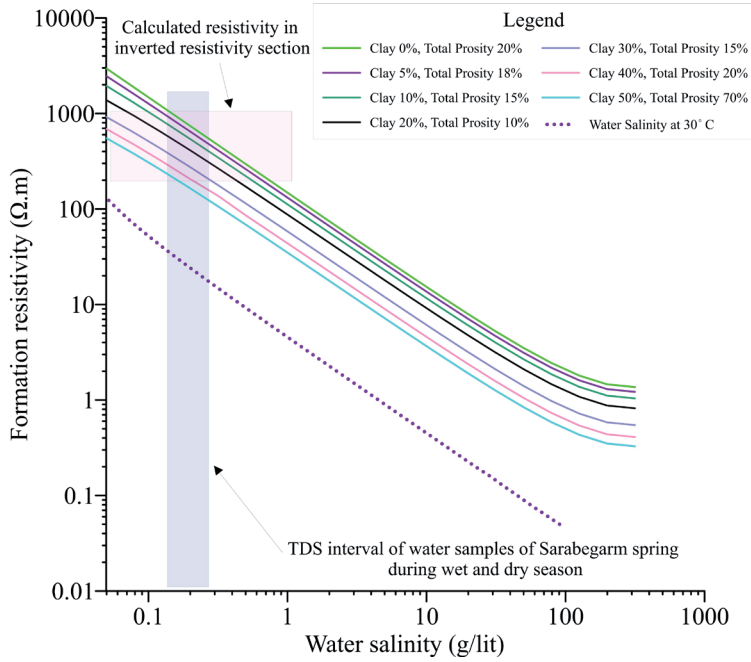


Fig. 7 - Theoretical resistivity-porosity cross-plots for limestone belonging to the Asmari Formation based on the petrophysical parameters of the Asmari Formation.

was dissected by the F3 fracture at its SW end. Water could initially flow along the F3 fracture and, then, be channelled into the F4 fracture and, finally, emerge through the Sarabegarm spring.

Protecting the catchment area above the Sarabegarm spring from animals and humans is important to prevent contamination. Fractures usually provide high permeability in the limestone, allowing deep drainage of water into the karst aquifer. Results of this study show that the traces of the F3 and F4 fractures have potential to be related to the main karst conduit of the Sarabegarm spring. Therefore, ideally an area leaving a minimum distance of 50 m near these fractures traces should be fenced to prevent any human activity and animal grazing. Also, surface runoff should be directed to an area outside these fractures. The local community and users of the spring should be instructed concerning the protection of this area above the spring.

## 6. Conclusions

The Sarabegarm spring is the main discharge zone of the Asmari aquifer. It is not possible to find the exact location and depth of the main conduit system near the spring only by the surface investigations. The MALM is a good method to find general groundwater flow direction since its relatively fast acquisition rates enable gathering spatial data in an almost non-invasive and cost-effective manner. Under favourable circumstances, the MALM can be used to satisfactorily map mostly probable groundwater flow toward springs. However, its performance can be significantly limited by the common occurrence of low signal-to-noise ratios due to the electromagnetic noise and electromagnetic coupling effect during the survey.

In this study, a higher signal-to-noise ratio was achieved with the use of frequency domain resistivity measurements with a frequency equal to 0.61 Hz. The resulting normalised iso-

potential contour showed that the groundwater flow towards the Sarabegarm spring followed a N25E trend. That direction coincided with the traces of the F4 and F5 fractures.

Results of the MALM, as expected, indicate the approximate location of conduits while providing no information on their depth and shape. In turn, the 2D resistivity and chargeability sections offered depth distribution of resistivity and chargeability values.

In order to receive high quality resistivity and chargeability data especially in noisy environments, resistivity and chargeability were measured with frequency domain (in frequency 0.61 Hz) and phase-frequency (in frequencies of 0.61 and 2.44 Hz) methods. Since the noises are site dependent, the use of the 0.61 Hz frequency is valid in the current case study and may not be generalised. Based on the statistical analysis of inverted resistivity value, the resistivity less than 100 Ω·m and more than 200 Ω·m was, respectively, related to the alluvium and limestone. The only notable result in the chargeability section was a distinction between the fine grain sediment from the courser one in alluvium.

Theoretical cross-plots of porosity-resistivity curves, produced to analyse petrophysical properties of limestone accurately, showed that resistivity of bulk limestone with total porosity of 20% in saturated conditions (by groundwater with TDS value between 160 to 250 mg/l), could not be decreased up to 200 Ω·m (as observed in Zone 2). Furthermore, no anomalous chargeability value showed the presence of minor clay or silt in some parts of limestone. Therefore, the decrease in the resistivity value was most probably due to the increase in the secondary porosity of limestone. In addition, resistivity values greater than 2,000 Ω·m were related to a relict conduit (Zone 4).

Comparing the results of the MALM and 2D resistivity and chargeability sections showed that the coincidence of a low resistivity value in the resistivity section (Zone 2) with a direction of groundwater flow toward the Sarabegarm spring. This zone also coincides with surface trace of the F4 fracture. From the contamination point of view, the area between the S66 to S81 stations on the resistivity profile, together with the through surface traces of the F3, F4, and F5 fractures, have the highest vulnerability and must be protected from any activity posing a risk of contamination.

**Acknowledgments.** The authors greatly appreciate the cooperation of the ZAP Company for providing facilities and useful data. The authors would also like to thank the University of Tehran for providing facilities and the leave time to work on this research.

REFERENCES

Al-Fares W., Bakalowicz M., Guerin R. and Dukhan M.; 2002: *Analysis of the karst aquifer structure of the Lamalou area (Herault, France) with ground penetrating radar*. J. Appl. Geophys., 51, 97-106, doi: 10.1016/S0926-9851(02)00215-X.

Alija S., Torrijo F.J. and Quinta-Ferreira M.; 2013: *Geological engineering problems associated with tunnel construction in karst rock masses: the case of Gavarres tunnel (Spain)*. Eng. Geol., 157, 103-111, doi: 10.1016/j.enggeo.2013.02.010.

Bakalowicz M.; 2005: *Karst groundwater: a challenge for new resources*. Hydro. J., 13, 148-160, doi: 10.1007/s10040-004-0402-9.

Beres J.; 2013: *Characterization of anisotropy in a karstified carbonate platform using seismic and electrical resistivity methods: a joint approach.* Ph.D. Thesis in Earth Science, Université Paris Sud-Paris XI, Paris, France, 177 pp.

Chalikakis K., Plagnes V., Guerin R., Valois R. and Bosch F.P.; 2011: *Contribution of geophysical methods to karst-system exploration: an overview*. Hydrol. J., 19, 1169-1180, doi: 10.1007/s10040-011-0746-x.

Cheng Q., Chen X., Tao M. and Binley A.; 2019: *Characterization of karst structures using quasi-3D electrical resistivity tomography*. Environ. Earth Sci., 78, 285, doi: 10.1007/s12665-019-8284-2.

Debeglia N., Bitri A. and Thierry P.; 2006: *Karst investigations using microgravity and MASW; application to Orléans, France*. Near Surf. Geophys., 4, 215-225, doi: 10.3997/1873-0604.2005046.

Ford D. and Williams P.D.; 2007: *Karst hydrogeology and geomorphology*. John Wiley & Sons, Hoboken, NJ, USA, 576 pp.

Gan F., Han K., Lan F., Chen Y. and Zhang W.; 2017: *Multi-geophysical approaches to detect karst channels underground - A case study in Mengzi of Yunnan Province, China*. J. Appl. Geophys., 136, 91-98, doi: 10.1016/j.jappgeo.2016.10.036.

Green R.T., Painter S.L., Sun A. and Worthington S.R.H.; 2006: *Groundwater contamination in karst terranes*. Water, air & soil pollution. Focus, 6, 157-170, doi: 10.1007/s11267-005-9004-3.

Hunter J.A.M. and Crow H.L. (eds); 2015: *Shear wave velocity measurement guidelines for Canadian seismic site characterization in soil and rock*. Nat. Resour. Canada, 226 pp., doi: 10.4095/297314.

Iran Meteorical Organization; 2020: < http://www.irimo.ir >.

Iran Water Resources Management Company; 2020: < https://www.wrm.ir >.

Iranian National Oil Company; 2006: *Geological quadrangle map of Sarpolezahab, with explanatory text in Persian*. Scale: 1:100,000, 1 sheet.

Kalhor K., Ghasemizadeh R., Rajic L. and Alshawabkeh A.; 2019: *Assessment of groundwater quality and remediation in karst aquifers: a review*. Groundwater Sustainable Dev., 8, 104-121, doi: 10.1016/j.gsd.2018.10.004.

Kulikov A.V. and Shemyakin E.A.; 1978: *Geoelectric prospecting using phase method of induced polarization*. Nedra press, Moscow, 157 pp. in Russian.

Kulikov V.A., Gruzdeva I.D. and Yakovlev A.G.; 2013: *A VES-IP survey near the geophysical station of Moscow State University, in the Kaluga region*. Moscow Univ. Geol. Bull., 68, 191-199, doi: 10.3103/S0145875213030034.

Li G., Goldscheider N. and Field M.S.; 2016: *Modeling karst spring hydrograph recession based on head drop at sinkholes*. J. Hydrol., 542, 820-827, doi: 10.1016/j.jhydrol.2017.12.021.

Loke M.H.; 2010: *Tutorial: 2-D and 3-D electrical imaging surveys.* Geotomo Software Inc., Houston, U.S.A., 128 pp.

Martin J.B. and Screaton E.J.; 2001: *Exchange of matrix and conduit water with examples from the Floridan Aquifer*. In: Kuniansky E.L. (ed), U.S. Geological Survey, Karst Interest Group Proceedings, Water-Resources Investigations, Reston, VA, USA, Report 01-4011, pp. 38-44, doi: 10.1016/S0009-2541(01)00320-5.

McGrath R.J., Styles P., Thomas E. and Neale S.; 2002: *Integrated high-resolution geophysical investigations as potential tools for water resource investigations in karst terrain*. Environ. Geol., 42, 552-557, doi: 10.1007/s00254-001-0519-2.

Milanović P.; 2018: *Engineering karstology of dams and reservoirs*. CRC Press, Boca Raton, FL, USA, 355 pp.

Miliaresis G.C.; 2001: *Geomorphometric mapping of Zagros ranges at regional scale*. Comput. Geosci., 27, 775-786, doi: 10.1016/S0098-3004(00)00168-0.

Moore D.L. and Stewart M.T.; 1983: *Geophysical signatures of fracture traces in a karst aquifer (Florida, U.S.A.)*. J. Hydrol., 61, 325-340, doi: 10.1016/0022-1694(83)90256-1.

Mozafari M. and Raeisi E.; 2015: *Understanding karst leakage at the Kowsar Dam, Iran, by hydrogeological analysis.* Environ. Eng. Geosci., 21, 325-339, doi: 10.2113/gseegeosci.21.4.325.

Mozafari M. and Raeisi E.; 2016: *Salman Farsi Dam reservoir, a successful project on a karstified foundation, SW Iran*. Environ. Earth Sci., 75, 1044, doi: 10.1007/s12665-016-5844-6.

Mozafari M., Raeisi E. and Guerrero J.; 2018: *Contribution of spectral coherency analysis and tracer test to study leakage at the Doosti Dam reservoir, Iran and Turkmenistan*. Environ. Earth Sci., 77, 139, doi: 10.1007/s12665-018-7326-5.

Mozafari M., Milanović P. and Jamei J.; 2021: *Water leakage problems at the Tangab Dam reservoir (SW Iran), case study of the complexities of dams on karst*. Bull. Eng. Geol. Environ., 80, 7989-8007, doi: 10.1007/s10064-021-02387-z.

Palmer A.N.; 1991: *Origin and morphology of limestone caves*. Geol. Soc. Am. Bull., 103, 1-21.

Pant S.R.; 2004: *Tracing groundwater flow by mise-a-la-masse measurement of injected saltwater*. J. Environ. Eng. Geophys., 9, 155-165, doi: 10.4133/JEEG9.3.155.

Pazzi V., Di Filippo M., Di Nezza M., Carlà T., Bardi F., Marini F., Fontanelli K., Intrieri E. and Fanti R.; 2018: *Integrated geophysical survey in a sinkhole-prone area: microgravity, electrical resistivity tomographies, and seismic noise measurements to delimit its extension*. Eng. Geol., 243, 282-293, doi: 10.1016/j.enggeo.2018.07.016.

Redhaounia B., Ilondo B.O., Gabtni H., Sami K. and Bédir M.; 2016: *Electrical Resistivity Tomography (ERT) applied to Karst carbonate aquifers: case study from Amdoun, northwestern Tunisia*. Pure Appl. Geophys., 173, 1289-1303, doi: 10.1007/s00024-015-1173-z.

Ryjov A.A. and Sudoplatov A.D.; 1990: *The calculation of specific electrical conductivity for sandy-clayed rocks and the usage of functional cross-plots for the decision of hydrogeological problems*. In: Scientific and Technical Achievements and Advanced Experience in the Field of Geology and Mineral Deposits Research, Moscow, Russia, pp. 27-41, in Russian.

Saein A.F. (ed); 2018: *Tectonic and structural framework of the Zagros Fold-Thrust Belt, Vol. 3, 1 ed*. Elsevier, Amsterdam, The Netherlands, 310 pp.

Shevnin V., Delgado-Rodríguez O., Mousatov A. and Ryjov A.; 2006a: *Estimation of soil superficial conductivity in a zone of mature oil contamination using DC resistivity*. In: Proc. 19th EEGS Symposium on the Application of Geophysics to Engineering and Environmental Problems 2006, Seattle, WA, USA, pp. 1514-1523, doi: 10.4133/1.2923613.

Shevnin V., Delgado Rodríguez O., Mousatov A., Flores Hernandez D., Zegarra Martínez H. and Ryjov A.; 2006b: *Estimation of soil petrophysical parameters from resistivity data: application to oil-contaminated site characterization*. Geofís. Int., 45, 179-193.

White W.B.; 2007: *A brief history of karst hydrogeology: contributions of the NSS*. J. Cave Karst Stud., 69, 13-26, doi: 10.4133/1.2923613.

Wightman W.E., Jalinoos F., Sirles P. and Hanna K.; 2003: *Application of geophysical methods to highway related problems*. Federal Highway Administration, Central Federal Lands Highway Division, Lakewood, CO, USA, FHWA-IF-04-021, 742 pp.

Worthington S.R.H.; 1999: *A comprehensive strategy for understanding flow in carbonate aquifers*. In: Palmer A.N., Palmer M.V. and Sasowsky I.D. (eds), Karst modelling, Karst Waters Institute, Charles Town, WV, USA, Special Publication, Vol. 5, pp. 30-37.

Zarroca M., Comas X., Gutiérrez F., Carbonel D., Linares R., Roqué C., Mozafari M., Guerrero J. and Pellicer X.M.; 2017: *The application of GPR and ERI in combination with exposure logging and retrodeformation analysis to characterize sinkholes and reconstruct their impact on fluvial sedimentation*. Earth Surf. Processes Landforms, 42, 1049-1064, doi: 10.1002/esp.4069.

Zhu J., Currens J.C. and Dinger J.S.; 2011: *Challenges of using electrical resistivity method to locate karst conduits - A field case in the Inner Bluegrass region, Kentucky*. J. Appl. Geophys., 75, 523-530, doi: 10.1016/j.jappgeo.2011.08.009.

Zonge K., Wynn J. and Urquhart S.; 2005: *Resistivity, induced polarization and complex resistivity*. In: Butler D.K. (ed), Near-Surface Geophysics, Society of Exploration Geophysicists, Tulsa, OK, USA, pp. 265-300, doi: 10.1190/1.9781560801719.ch9.

*Corresponding author:* Morteza Mozafari
School of Geology, College of Science, University of Tehran
16 Azar Street, Tehran, Iran
Phone: +98 2161112906; e-mail: mmozafari@ut.ac.ir